GCAGS JOURNAL
A Publication of the Gulf Coast Association of Geological Societies
www.gcags.org

Textures, Mineralogy, and Reservoir Properties of an Altered Mafic Tuff Core from the Upper Cretaceous (Lower Campanian) of Central Texas

Robert M. Reed and Robert G. Loucks

Bureau of Economic Geology, Jackson School of Geosciences, University of Texas at Austin, Box X, University Station, Austin, Texas 78713–8924, U.S.A.

ABSTRACT

The Upper Cretaceous Balcones Igneous Province of Central and South Texas includes volcanic deposits (mounds) of tuffaceous rocks, and, where shallowly buried, these tuff mounds have high porosities, so some mounds have proven to be oil reservoirs. In this study, a core from the Ballard #2–C well, Dale Field, Caldwell County, Texas, has been investigated for fabric, texture, mineralogy, porosity, and permeability. Extensive alteration has not erased much of the original igneous texture and fabric, but volcanic glass and phenocrysts have been largely altered, primarily to interlayered smectite/vermiculite. Extensive cementation by a variety of minerals has also reduced porosity. Mean porosity of the samples measured is 28.8%. Pores are present predominantly in four locations: between lapilli (interparticle), in partly replaced dissolved phenocrysts (intraparticle), in partly cemented vesicles (intraparticle), and between phyllosilicates replacing volcanic glass (intraparticle). Pore sizes extend from nanometers to millimeters in diameter. Measured permeabilities range from <1 md to 6 md, although the values may be high because of postcoring microfractures in sample plugs. The core has few natural macrofractures and little fracture porosity. Mercury-injection capillary-pressure tests show that most pore throats are <250 nm in diameter, forming a nano- to micropore system. Nuclear magnetic resonance scans also show a predominance of nanometer-scale pores. Given observed properties, the tuff studied should have high storage capabilities (i.e., pore volume) but low permeability.

INTRODUCTION

Occurrences of hydrocarbons in igneous rocks have been noted for decades (e.g., Shuster et al., 2021), and Central and South Texas have examples of these reservoirs (e.g., Ewing and Caran, 1982) that are in many ways atypical of other igneous rock reservoirs, which commonly rely on open fractures for productivity rather than matrix (i.e., nonfracture) pores. This study delineates some of the reservoir properties of one volcanic core from a suite of volcanic rocks that produce hydrocarbons in the Balcones Igneous Province. The study had the following objectives: (1) core description of texture, fabric, and sedimentary features; (2) petrographic analyses at a variety of scales; and (3) analysis of petrophysical measurements to explain reservoir properties. This investigation is the only published, modern, detailed investigation of the reservoir properties of a volcanic-mound producing reservoir in the Balcones Igneous Province.

Manuscript received May 17, 2022; revised manuscript received July 27, 2022; manuscript accepted July 27, 2022.

GCAGS Journal, v. 11 (2022), p. 1–15.

GEOLOGIC BACKGROUND

The Upper Cretaceous Balcones Igneous Province of Central Texas (Figs. 1 and 2) is composed of a suite of silica-undersaturated, alkalic igneous rocks including >200 occurrences of both shallowly intrusive and extrusive (mostly tuffaceous) igneous rocks (Lonsdale, 1927; Spencer, 1969; Ewing and Caran, 1982; Barker et al., 1987; Griffin et al., 2010).

The extrusive rocks occur primarily as thick mounds of lapilli tuff (>2 mm particles) generated by mostly submarine volcanoes (Barker and Young, 1979; Ewing and Caran; 1982; Ewing, 1986), which can build up and become emergent with continued eruption. The lapilli tuffs are notable for having large numbers of inter- and intraparticle pores, despite extensive alteration and cementation. Tuff mounds are thickest at crater centers, which excavate (i.e., form cavities) into underlying strata and thin progressively toward the outer margins. Mound thicknesses including crater depth of as much as 1039 ft (316.7 m) have been observed (Thompson, 2019, his figure 6), but average thicknesses of a few hundred feet (100 m) are more common (e.g., Ewing and Caran, 1982; Thompson, 2019). Tuff accumulations are circular to slightly oval in plan view and have a diameter of up to several kilometers (a few miles) (Sellards, 1932; Ewing and Caran, 1982; Thompson, 2019). A slight southwest-northeast elongation of many of the mounds has been ascribed to either north-

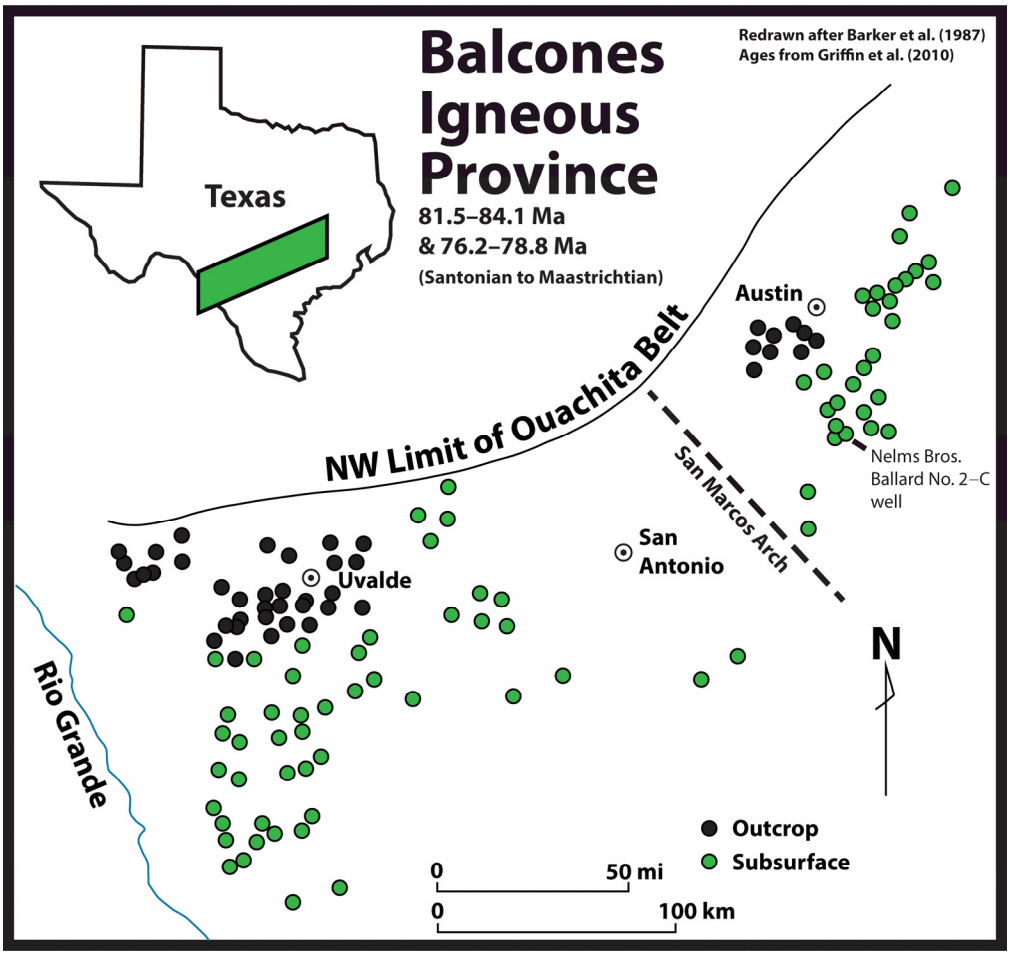

Figure 1. Map showing Balcones Igneous Province in Texas (modified after Barker et al. [1987]).

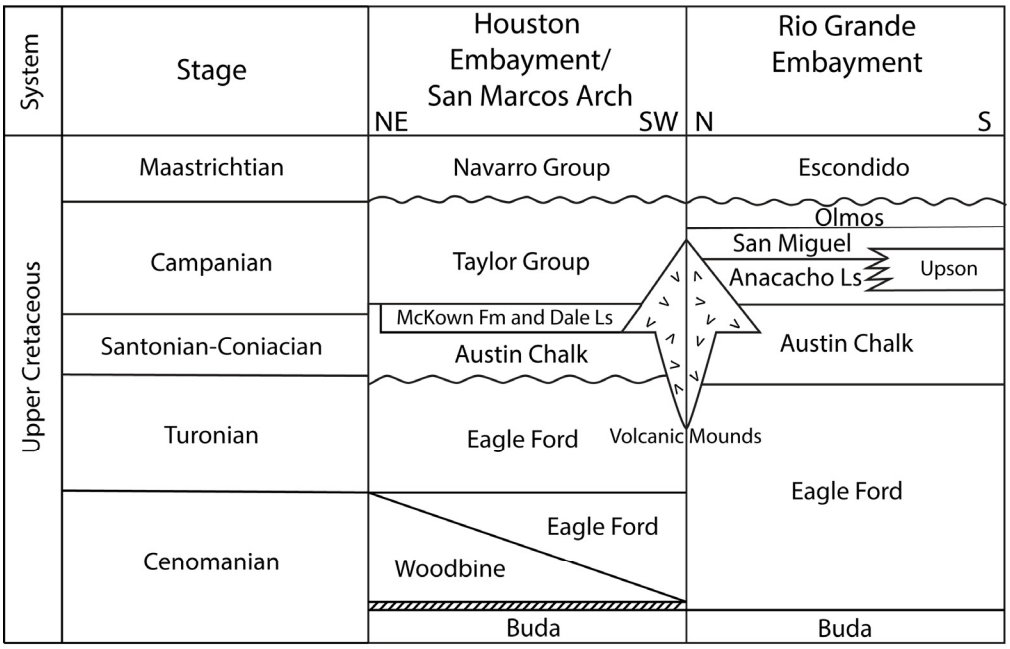

Figure 2. Stratigraphic column of Cretaceous of Central Texas showing position of volcanic rocks relative to associated units.

Based on Condon and Dyman (2006), Phelps et al. (2013), and M. E. Thompson (2022, pers. comm.)

east winds or currents (Ewing and Caran, 1982). An association of mound locations with northeast-trending faults of the Balcones-Luling Fault Zone has been previously suggested (Ewing and Caran, 1982) (Fig. 3). Deeper basement faults may have played a role in localizing magma access to the surface.

Volcanic mounds occur within Upper Cretaceous Austin Chalk and Taylor (Anacacho) strata (Ewing and Caran, 1982), primarily deepwater carbonates and calcareous mudstones (e.g., Loucks et al., 2020). The mounds have been a hydrocarbon drilling target since 1915 (Udden and Bybee, 1916; Sellards, 1932). Different volcanic centers were active at different times (Griffin et al., 2010; Thompson, 2019), with some appearing to be contemporaneous with deposition of the upper units of the Upper Cretaceous Austin Chalk (Barker and Young, 1979; Loucks and Reed, 2022) and others appearing to be contemporaneous with deposition of the Upper Cretaceous Taylor Clay (Anacacho) (Udden and Bybee, 1916; Sellards, 1932). Correlations are complicated because the explosive submarine (phreatomagmatic) volcanism that formed the volcanic mounds also excavated wide craters into underlying, partly consolidated strata (Ewing and Caran, 1982; Thompson, 2019), such as the Upper Cretaceous Eagle Ford Group (Fig. 2). See Loucks and Reed (2022) for a diagrammatic representation of the stages of volcanic-mound development.

With only a limited number of precise radiometric-age dates (three for the mafic part of the suite and five for the felsic part of the suite; Griffin et al., 2010), controversy remains on the age range represented by these intrusions (Thompson, 2019). Study of the Upper Cretaceous Austin Chalk (Loucks and Reed, 2022) suggests that most volcanic activity during Austin Chalk time was concentrated during the time of the AC–B1 subunit (i.e., lowermost Campanian upper Austin Chalk). However, a range in timing of eruptions from early Austin Chalk time to well into the Taylor/Anacacho appears most likely.

Many volcanic mounds have related occurrences of shallow-water carbonates (e.g., the McKown Member and the Dale Limestone), unlike those of the deeper water Austin Chalk (Luttrell, 1977; Thompson, 1986; Loucks and Reed, 2022). The elevated mounds provided shallow-water settings where the carbonate factory was able to produce abundant carbonate material in atolls rimming mounds and shoals on submerged mounds.

These volcanic mounds are readily imaged using seismic and magnetic techniques (Ogiesoba and Eastwood, 2013; Ogiesoba and Klokov, 2017), as well as by detailed wireline correlations (Thompson, 2019). Where available, seismic imaging provides a clear method of defining three-dimensional morphology of the volcanic mounds.

Previous researchers (e.g., Lonsdale, 1927; Spencer, 1969; Barker et al., 1987) noted a range of alkalic silica-undersaturated compositions in associated intrusive igneous rocks, and it is thought that the associated extrusive rocks including the tuffs will show a similar range of compositions. Some previous researchers (e.g., Udden and Bybee, 1916) mistakenly characterized the tuffs as being predominantly serpentine, although none of the serpentine group minerals occurs as the dominant alteration product of these tuffs.

DATA AND METHODS

This study investigated a core from a tuff mound in the north part of the province (Caldwell County, Fig. 3) taken from the Nelms Brothers #2–C Ballard well in Dale Field. In analyses of samples from the core, we examined texture and fabric, mineralogy, porosity, permeability, and mercury capillary injection pressure (MICP). Core depth ranges from 2215 to 2295 ft (80 ft interval) (675.1 to 699.5 m [24.4 m interval]), and the tuff is underlain by Upper Cretaceous Austin Chalk and overlain by a thin layer of the Dale Lime Member and then Upper Cretaceous Taylor Marl (Thompson, 2019, his figure 3). Examination of wireline logs as interpreted by Thompson (2019, his figure 3) shows that the tuff section is ~600 ft (182.9 m) thick in this area, given data from the nearby Nelms Brothers #1 Ballard well. Core in the #2–C Ballard was taken from the tuff 300 ft (91.4 m) below the capping Dale Lime (M. E. Thompson, 2022, pers. comm.). Initial production from the well is reported as 21 BOPD (M. E. Thompson, 2022, pers. comm.), the core being taken from just beneath the interval that was ultimately perforated and produced. Core was visually described and logged at a 1 in = 1 ft scale, with core logging including texture and fabric, depositional and structural features, cements, macropores, and macrofractures. On the basis of lithologies noted during core logging, 13 samples for polished thin sections were selected, eight of which were prepared from the end trims of core plugs to equate petrographic description directly to petrophysical analyses. Samples were impregnated with blue-dyed epoxy to facilitate viewing of macropores in thin section, and they were also impregnated with blue-fluorescent dye to detect nano- and micropores under UV light. UV analysis indicated that the matrix is tight, so epoxy was limited to only partial impregnation of the matrix, penetrating only the edges of plugs or along induced microfractures.

On the basis of differences in visual characteristics of the core, eight representative core plugs were analyzed for helium porosity and permeability at Weatherford Laboratories in Midland, Texas (Table 1).

Nuclear magnetic resonance (NMR) and MICP measurements were made on three plug samples showing a range of values (Table 1) by Core Laboratories in Houston, Texas.

High-resolution X–ray computed tomography (CT) was conducted on the most permeable and least permeable (as measured) of the core-plug samples by the University of Texas at Austin Computed Tomography Laboratory (UTCT). Voxel size for CT scans is 13.2 µm, and samples were done as a helical continuous CT scan on an NSI scanner with a Fein focus high-power source (170 kV, 0.19 mA) and a Perkin Elmer detector.

Two chip samples were selected for scanning electron microscope (SEM) examination of broken surfaces. Two samples were also prepared using broad ion-beam milling with Ar ions for SEM examination of micro- and nanopores. Samples were processed using a Leica EM Triple Ion-Beam Cutter system, and ion milling was done using an accelerating voltage of 8 kV, a source current of 2.8 mA, and a milling time of 10 h. Milled samples were given an ~6 nm coating of iridium to prevent charge buildup during SEM examination. Several polished thin sections were also selected for examination of texture and mineralogy in the SEM. Polished thin sections were given a 25 nm coat of carbon before examination. SEM samples were imaged using a field-emission SEM; an FEI Nova NanoSEM 430 model equipped with dual Bruker XFlash® SDD energy dispersive spectroscopy (EDS) systems for element identification and mapping. A moderate accelerating voltage of 15 kV was used on this system to avoid electron-beam damage to the samples while still allowing EDS mapping. SEM working distances for imaging were ~6 mm and for EDS mapping were 9 to 10.5 mm. Both SEM images and EDS element maps were collected from all samples. Backscattered electron images acquired were useful in differentiating textures.

Three samples of varying lithologies were selected and sent to QMinerals BV (Heverlee, Belgium) for quantitative X–ray diffraction analysis. Sample preparation for bulk analysis was by wet milling and spray drying, and the diffractometer was a Bruker D8 Advance using an XE–T detector and Cu–Kα radiation. Detailed clay analysis involved chemical pretreatment to remove cementing agents, followed by extraction of the <2 µm fraction by sequential centrifugation. Oriented clay slides were recorded in air-dry and ethylene glycol conditions.

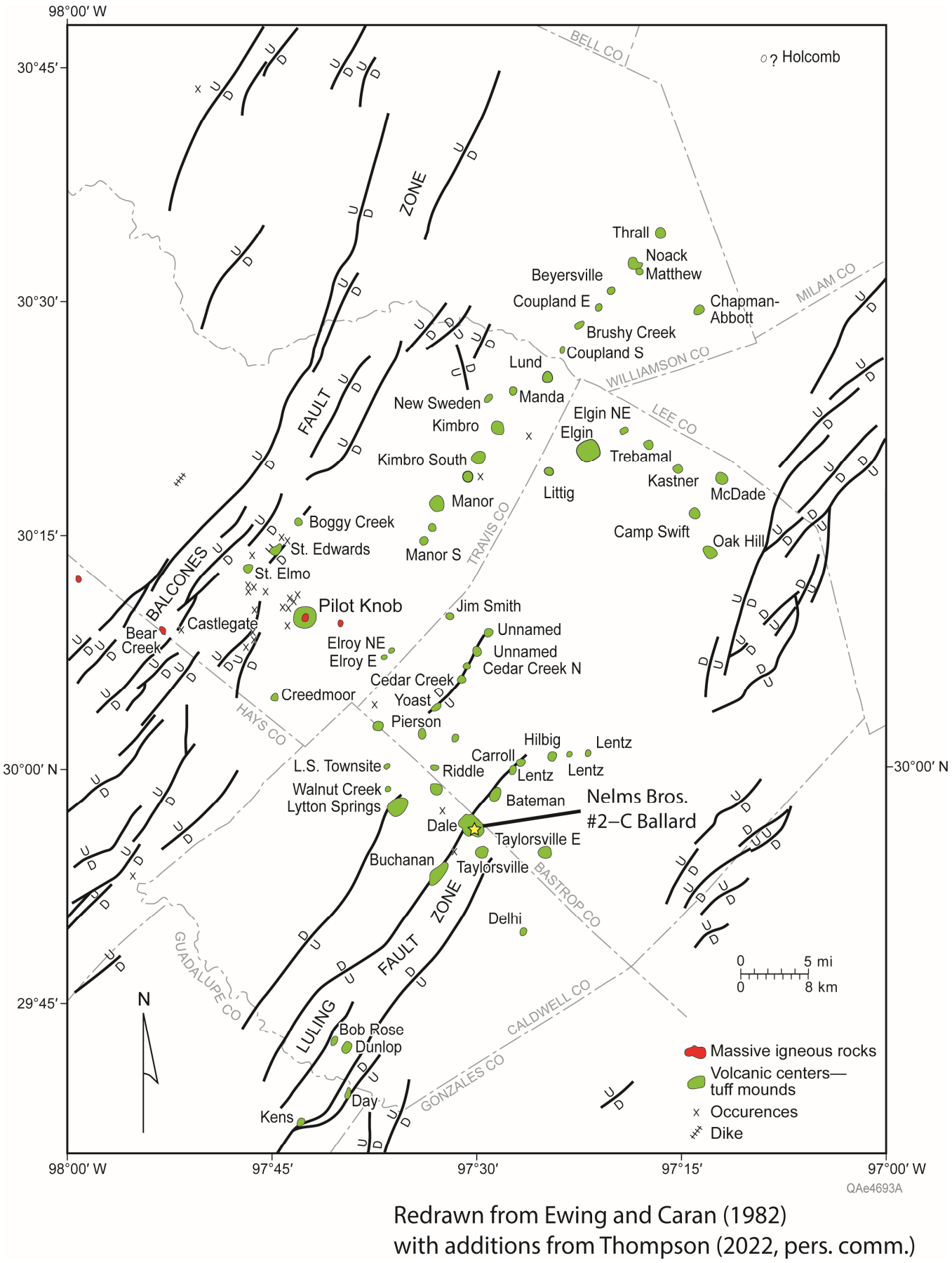

Figure 3. Map showing north part of Balcones Igneous Province and location of the Nelms Brothers #2–C Ballard well. Redrawn from Ewing and Caran (1982).

TEXTURES, MINERALOGY, AND ALTERATION

Core lithology is variable at inch (centimeter) scale, which requires it to be visually described at a high resolution. Most particles are fine lapilli (i.e., >2 mm in diameter), although finer ash grains are also present. In some poorly cemented layers, macropore space is visible between lapilli. Sporadic layering (bedding) within cores is defined primarily by differences in cementation, particularly of bladed white cements (discussed later) (e.g., Fig. 4A), which are assumed to reflect original depositional layering. Some fainter beds are defined by a slight change in grain size (Fig. 4B). Bedding can be inclined in the core, and inclination can vary in direction (Fig. 4C). In some cases, this variation is in continuous lengths of core, so it is known to be an actual change in dip direction. Steeply inclined bedding in some intervals suggests slumping of material prior to lithification (Figs. 4A–4C). Graded bedding was not observed nor were packages of deposition apparent. Near vertical stringers of cement are present in a few sections of core (Fig. 4D), probably representing tilted blocks.

A few small, possibly chalky, xenoliths were noted in this core, and a few autoliths of tuffaceous material of a slightly different composition and texture were noted (Fig. 5). Autolith size ranges from <1 cm to several centimeters in diameter, indicating some recycling of volcanic material during prolonged phreatomagmatic eruptions.

Tuffs are mafic in composition and have an extremely complex mineralogy reflecting original igneous compositions heavily overprinted by devitrification, alteration, and cementation (Table 2). Mineralogy of the tuffs is more fully examined in a forthcoming manuscript by our research group. The dominant mineral of these samples, according to XRD (Table 2) and SEM analyses, is a complex interlayered clay that we term interlayered vermiculite/smectite for this investigation. On the basis of EDS analysis showing increased Na in rimming clay cements, we conclude that these later cements have more of a smectite component.

Two rarely occurring alteration minerals, pectolite (a hydrous Ca–Na–silicate) and xonotlite (a hydrous Ca–silicate), make up most of the white cement visible in core. Pectolite and xonotlite are both bladed, white, authigenic minerals that are difficult to differentiate from one another visually but are distinct chemically. Pectolite is more common in samples that have been examined. Minor amounts of blocky white calcite cement are present with the pectolite and xonotlite in some samples.

Smectite and interlayered smectite-vermiculite form both as alteration products of volcanic glass and as lapilli-rimming and vesicle-filling cements. On the basis of observed textural relations, we have found that vermiculite and smectite were early cements, followed in some samples by pectolite, xonotlite, and calcite.

Many subcentimeter-scale volcanic features are preserved in the tuffs, despite widespread alteration. CT scans (Fig. 6) and thin sections provide straightforward evidence of volcanic textures. Outlines of lapilli and ash (original volcanic grains of assorted sizes) are visible in all samples (Fig. 6). Samples are a poorly sorted mixture of generally subrounded lapilli and ash grains. In some sections of the core, a subtle, preferred orientation of slightly elongate grains defines a faint fabric as well. However, postdepositional deformation of the lapilli themselves does not appear to be common.

Most original volcanic minerals and volcanic glass are altered primarily to smectite and/or interlayered vermiculite-smectite or, in some cases, various Ca–Ti silicates and phosphate. Phenocrysts, presumably of olivine and/or titanaugite pyroxene, are almost always completely replaced by phyllosilicates.

Alteration style and intensity vary between adjacent lapilli, suggesting differences in starting material and noncontemporaneous origins of grains (i.e., not simultaneous in overall eruption). Several textural features argue for possible noncontemporaneous origins of adjacent grains. Alteration of lapilli material to complex Ca–Ti minerals varies widely between adjacent grains (Fig. 6). The degree of vesicle development also varies between adjacent grains. Shape and size of altered phenocrysts also vary between grains. Variations in alteration and cementation between lapilli lead to differences in pore development and preservation, which are discussed later.

FRACTURES

Natural macrofractures in the core are relatively rare, only two macrofractures having been observed in this core. One nonintact fracture near the top of the core appears unmineralized, although it may be lined with microscopic smectite cement. This fracture is subvertical and appears for about 1 ft (0.3 m) in the core. The other macrofracture, filled with predominately blocky to bladed white cements, is oblique to the core and at least 1 ft in length. Thin-section analysis shows that this fracture is filled with blocky calcite, bladed pectolite, and blocky barite. Aperture varies irregularly along the length of the fracture from <1 mm to several millimeters. The abrupt variations of aperture in this feature suggest that it may actually be a small transtensional fault. Fracture pores are minor and generally on the micrometer scale.

POROSITY, PERMEABILITY, AND PORE SYSTEMS

Helium porosities from 1 in (2.54 cm) core plugs have a mean of 28.8% (Table 1) and range from 26.5 to 30.6%, highlighting the excellent hydrocarbon storage potential of these rocks. Observations across a variety of scales show that pores are present in four locations: between lapilli (interparticle, Fig. 7A), in partly replaced dissolved phenocrysts (intraparticle, Fig. 7B), in partly cemented vesicles (intraparticle, Fig. 7C), and between phyllosilicates replacing volcanic glass (intraparticle, Fig. 7D). Pore sizes extend from nanometers to millimeters in diameter.

Larger pore spaces, both between ash grains and lapilli and within vesicles, are lined with combinations of smectite, vermiculite, pectolite (a hydrous Na– and Ca–silicate), xonotlite (a hydrous Ca–silicate) and, rarely (in this core), calcite. Smectite and vermiculite infilling interparticle pore space and vesicles are commonly radial. Pectolite and xonotlite are bladed, and xonotlite can also be radial. Calcite is generally blocky. Because the #2–C Ballard core has relatively more Na, it has more smectite and pectolite (Na–bearing minerals) than do other tuff cores currently under study, which have less Na, and, hence, fewer smectite interlayers and more xonotlite than pectolite.

Although pore spaces between lapilli (Fig. 7A) are the largest (in some cases visible in core and millimeters in diameter), these spaces are generally partly to completely filled with various cements. The pores commonly have a triangular cross section. Cements (particularly bladed pectolite and xonotlite) can reduce these pores to a network of nanopores.

Pores in partly replaced original igneous phenocrysts (Fig. 7B) are of intermediate size but are generally in the range of millimeters to nanometers, depending on degree of replacement versus dissolution of the phenocrysts. A few phenocrysts of clinopyroxene remain partly unreplaced in some samples (Table 2).

Vesicles, circular to oval in cross-section voids (gas bubbles) originally enclosed in volcanic glass (Fig. 7C), were originally intraparticle pore space, but in many cases have been partly to entirely filled with posteruptive cement. These pores range in diameter from ~400 μm to nanometers (where mostly occluded by cement). Difference in the presence and abundance of vesicles between adjacent grains is an indication of the heterogeneity of volcanic grains. The degree of vesicle filling commonly varies between adjacent lapilli in a sample. To what degree the

Table 1. Measured helium porosity and permeability values.

Sample #	Depth (ft)	Grain Density	Porosity (%)	Permeability (md)	Sample Description	NMR + MICP	CT Scans
1	2219.3	2.91	29.9	6.201	slightly coarser grained	yes	yes
2	2225.5	2.89	28.7	4.202	strongly laminated		
3	2242.6	2.89	27.7	2.921	vertical cement trails	yes	
4	2251	2.91	28.8	1.859	moderate cement, lamination		
5	2254	2.92	28.9	0.744	low cement, faint lamination		
6	2258.1	2.91	26.5	1.106	heavily cemented		
7	2287	2.92	29.2	2.349	low cement		
8	2291.8	2.91	30.6	0.598	moderate cement	yes	yes
Means		2.91	28.8	2.498			

completely uncemented vesicles are connected to the effective pore systems of the rocks is unknown, but the lack of blue-dyed epoxy in a few of these when viewed in thin section suggests that some are poorly connected.

Pores between clay minerals replacing volcanic glass (Fig. 7D) are on average the smallest, down to nanometers in diameter, making SEM examination necessary to see these pores. The pores are interesting in that what is thought to be an originally mostly nonporous volcanic glass has developed pores during alteration.

Klinkenberg permeability values for a limited sample set are in the range of 0.6 to 6.2 md (Table 1; Fig. 8), and the geometric mean of the permeabilities is 4.39 md. The most porous sample of this set also has the lowest permeability measurement. A plot of porosity versus permeability does not show a clear trend (Fig. 8). Also, a plot of permeability versus depth shows a weak correlation (Fig. 9A), with permeability decreasing with depth, although porosity shows no clear relationship with depth (Fig. 9B). Over this limited depth range, no correlation with depth is expected relative to a change in burial parameters, such as temperature.

X–ray CT imaging of two of the core plugs shows a number of microfractures that partly traverse the core plugs (Fig. 6) and the other plugs also show some microfractures in thin section. Examination of these microfractures in thin section suggest that they are not naturally occurring. These postcoring, induced microfractures are probably responsible for the millidarcy-level permeability measurements recorded, and any analysis of permeability will result in an overestimation of permeability. The three samples chosen for NMR and MICP analysis were therefore based on measured permeabilities, which may not be related to the original pore system, but to artifacts developed within the samples.

NMR analyses show very similar results in pore-size populations (Fig. 10). Three populations being defined as nanopores between clays, intraparticle mesopores, and interparticle pores. NMR porosities are similar to measured core-plug He porosities (mean 28.9% vs. mean 29.4%, respectively, for the three plugs). Effective porosities from NMR are much lower than total porosities, as calculated from He porosities or NMR analyses (mean 2.8% vs. mean 28.9%/29.4%, respectively), indicating much of the pore system has poor connectivity. Overall, these volcanic strata in this core are a tight reservoir, and permeabilities measured by core-plug analysis are considered unreliable because millidarcy-level permeability values are not expected from effective porosities in a range of 2.8%.

In a plot of mercury-saturation curves of three of the volcanic samples (Fig. 11), the curves are nearly similar, with entry pressures of ~4000 psi (~27.6 MPa). These entry pressures are relatively high, indicating a pore network connected by very fine pore throats. The curves are generally flat and have constant gradients of between 10 and 80% saturation, suggesting similar pore-throat sizes in much of the sample. Calculated pore-throat radii from the MICP curves show that pore-throat size distribution is also similar and in the nanometer range. Most pore throats have a radius of <70 nm (Fig. 12). A matrix pore network having these nanometer-scale pore throats will equate to a low-permeability reservoir.

DISCUSSION

Although available core is not long enough for a definitive statistical analysis of the role of macrofractures in production, the presence of only two macrofractures in 80 ft (24.4 m) of core suggests that the cored horizon of the Dale mound is not extensively fractured. Production variability between wells drilled in the same tuff mound (e.g., Sellards, 1936; Thompson, 2019) suggests that fractures may play a role in some wells.

Microfractures visible in CT scans are more problematic (Fig. 6). The core plug with the highest measured permeability has numerous microfractures, which are probably influencing the measurement. This supposition is supported by a core plug with the highest porosity and highest median pore-throat radius having the lowest measured permeability. This plug has fewer microfractures visible in CT than the sample with the highest measured permeability. Measured permeability values should therefore be considered maximum possible values, and actual permeabilities are probably near the low end of the measured range (i.e., hundreds of microdarcys).

Low permeabilities and presence of abundant micropores and nanopores, but high overall porosity values, suggest that wells in these volcanic tuffs may produce prolifically, although

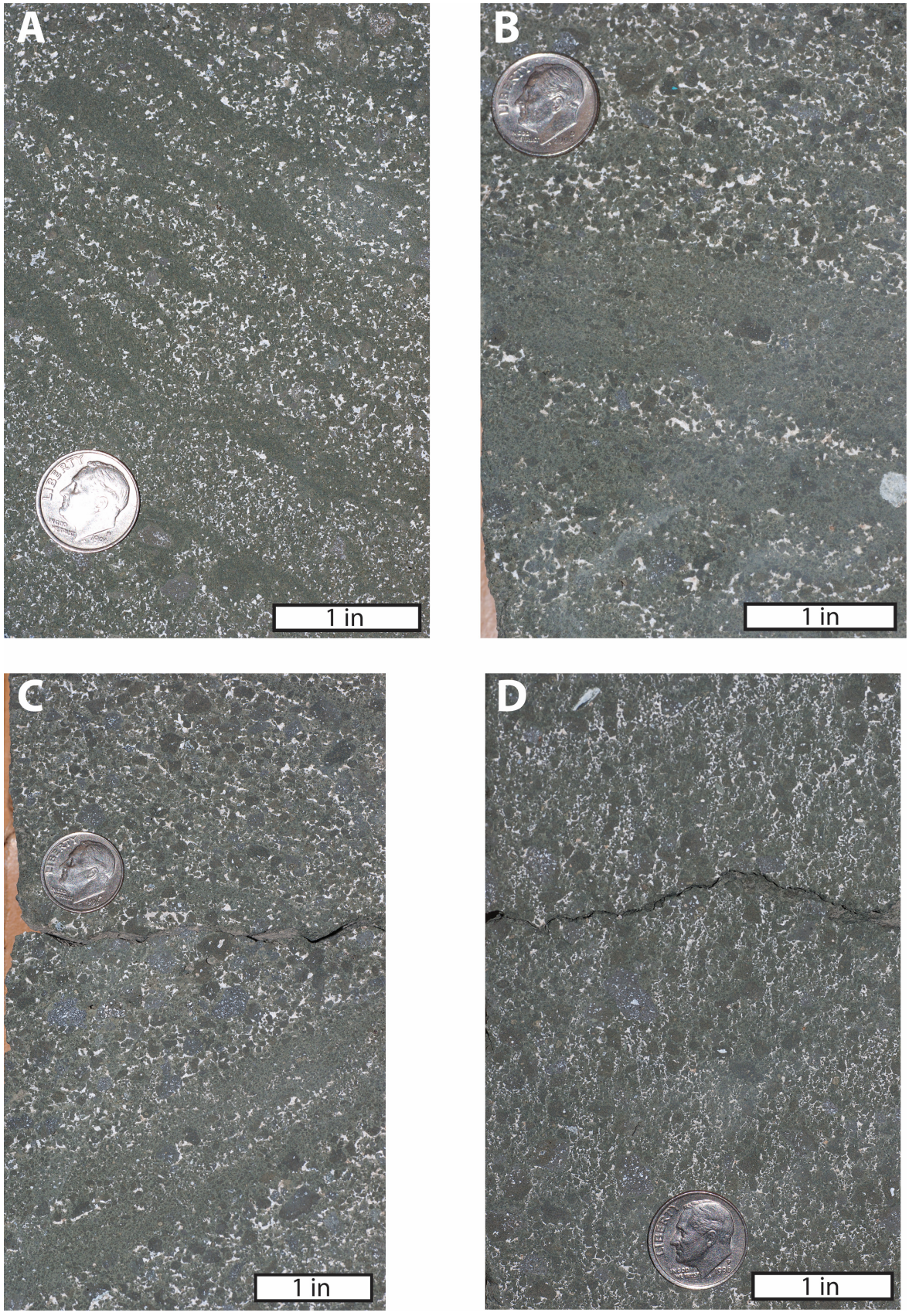

Figure 4. Photographs showing various textures in lapilli tuff cores. Diameter of coin, 18 mm for scale. (A) Inclined layering (bedding) defined by changes in composition of cement. Probably deposited on a steep slope. From 2225.2 ft (678.2 m). (B) Photograph showing layers partly defined by changes in grain size; greener layers have more ash; whiter layers have more lapilli. From 2250.0 ft (685.8 m). (C) Reversal in inclination of layering between top of picture and bottom of core section, perhaps related to slumping. From 2250.5 ft (686 m). (D) Vertical texture defined by white cement (mostly pectolite), probably a tilted block. From 2242.5 ft (683.5 m).

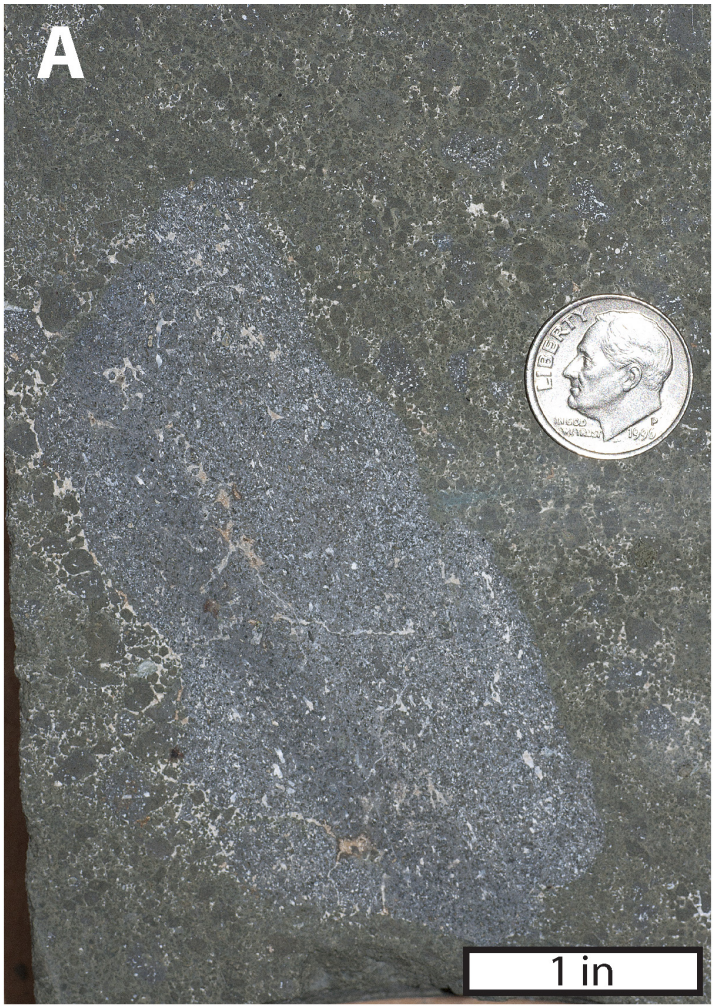

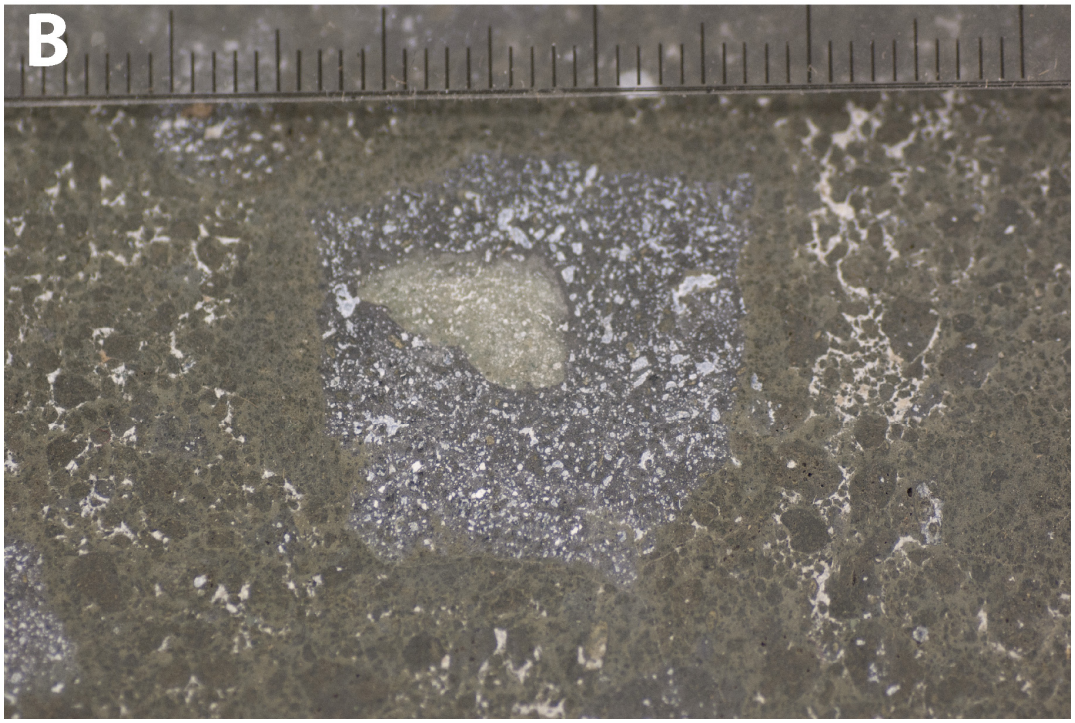

Figure 5. (A) Recycled volcanic autolith (volcanic block) containing layering found in massive lapilli tuff. Diameter of coin, 18 mm. From 2239 ft (682.4 m). (B) Recycled vesicular coarse lapilli containing even earlier recycled grain. Scale in millimeters. From 2280.7 ft (695.2 m).

Table 2. X–ray diffraction (XRD) results.

Mineral	Ballard, 2216.6 ft (675.6 m)	Ballard, 2219.3 ft (676.4 m)	Ballard, 2258.1 ft (688.3 m)
Pyroxene $Ca(Mg,Ti,Fe,Al)(Si,Al)_2O_6$	4.5	5.2	3.4
Schorlomite $Ca_3(Ti,Fe,Al)_2[(Si,Fe)O_4]_3$	2.5	1.4	1
Pectolite $NaCa_2Si_3O_8(OH)$	7.6	14.2	11.4
Calcite $CaCO_3$	1	0.1	0.7
Titanite $CaTi(SiO_4)O$	0	3.8	4.3
Apatite $Ca_5(PO_4)_3(OH,Cl,F)$	0	0.8	0.7
2:1 layer clays (Smectite/Vermiculite) $(K,Ca,Na)(Al,Mg,Fe)_2(Si,Al)_4O_{10}[(OH)_2,(H_2O)]$	83.8	74.1	78.1
Other	0.6	0.3	0.3
Total	100	99.9	99.9

slowly over a long well-production history. The original producing field from this play (Thrall Field in Williamson County, Texas; Fig. 3) is still producing minor, but economical, amounts of oil through secondary recovery via nitrogen injection (G. Pankonien, 2022, pers. comm.) after >100 yr.

Presence of smectitic clays in this core suggests that at least some of the volcanic mounds may be susceptible to swelling if freshwater is used in drilling, particularly because more smectitic clays tend to be late-stage cements lining pore space (i.e., in direct contact with induced fluids). Mounds having less Na–rich clays should have less smectite and possibly less chance of injection-fluid damage to the reservoir.

Volcanic mounds are present in more deeply buried areas of the Austin and Anacacho in South Texas, where they have been exploration targets (Ewing, 1986; Hutchinson, 1994). Given the clay-rich compositions and reactive nature of the tuffs, these mounds will have experienced higher temperatures and pressures and are likely to be less porous because of increased compaction and cementation.

CONCLUSIONS

In the Dale mound tuffs, widespread alteration has converted most original volcanic glass and primary igneous minerals to smectite and/or vermiculite plus complex Ca–Ti minerals. Some igneous titanaugite pyroxene and intermediate ferrochromite-spinel remain in a few samples. Despite widespread alteration, many volcanic textures such as vesicles and lapilli are preserved in the tuffs. Cements precipitating around lapilli and in vesicles include pectolite, xonotlite, vermiculite, smectite, calcite, barite, and minor Ca–phosphate. Not all cements are present in all samples.

Diagenesis and alteration have both created (e.g., dissolution of some phenocrysts) and destroyed (growth of pore-filling cements) pore space in these tuffs. Pores are common in four locations (Fig. 7): between lapilli, in partly dissolved and replaced phenocrysts, in partly cemented vesicles, and between phyllosilicates replacing volcanic glass. Fracture porosity is rare and minor in this core.

Porosities of a set of core plugs average 28.8%, with a high of 30.6% and a low of 26.5%. Permeability measurements were influenced by induced microfractures present in the cores. Lowest reported permeabilities, in the range of hundreds of microdarcys, are probably closest to being accurate.

Both MICP and NMR results for the three samples that were analyzed using these techniques are similar, despite variable measured permeabilities, and MICP shows that pore throats are dominated by nanometer-size throats. NMR shows that nanopores are the most abundant pores, with smaller numbers of pores in larger sizes.

Despite a long history of these tuff bodies being referred to as serpentine mounds, according to XRD and SEM EDS, little or no actual serpentine is present in this particular core. This fact has not proven to be the case in other tuff bodies in this trend, where minor serpentine has been found (Reed et al., 2022).

Overall, core from a reservoir in a volcanic tuff mound shows the reservoir to be relatively tight, but with good storage space, and although production rates are low, wells may have a long production history. More core description and analyses need to be completed to document reservoir properties and heterogeneity in other tuff mounds. This investigation is an initial contribution to the understudied reservoir properties of these volcanic-mound reservoirs.

ACKNOWLEDGMENTS

Funding for this study was supplied by the State of Texas Advanced Resource Recovery (STARR) Program at the Bureau of Economic Geology. Computed tomography data and images were produced at the High-Resolution X–Ray Computed Tomography Facility of the University of Texas at Austin, which is supported by the NSF Division of Earth Science Instrumentation and Facilities Program (NSF EAR–1762458). Mark Thompson, Tim Boardman, Tim Lawton, Bill Ambrose, and Rich Kyle are thanked for discussions on the tuffs and surrounding rocks. Rieko Adriaens is thanked for discussions regarding the XRD data. Reviews by Tom Ewing, Charlotte Sullivan, and Mark Thompson improved the manuscript. The Media Group at the Bureau of Economic Geology is thanked for graphics support. Technical editing was supplied by Lana Dieterich. Publication authorized by the Director, Bureau of Economic Geology, Jackson School of Geosciences, University of Texas at Austin.

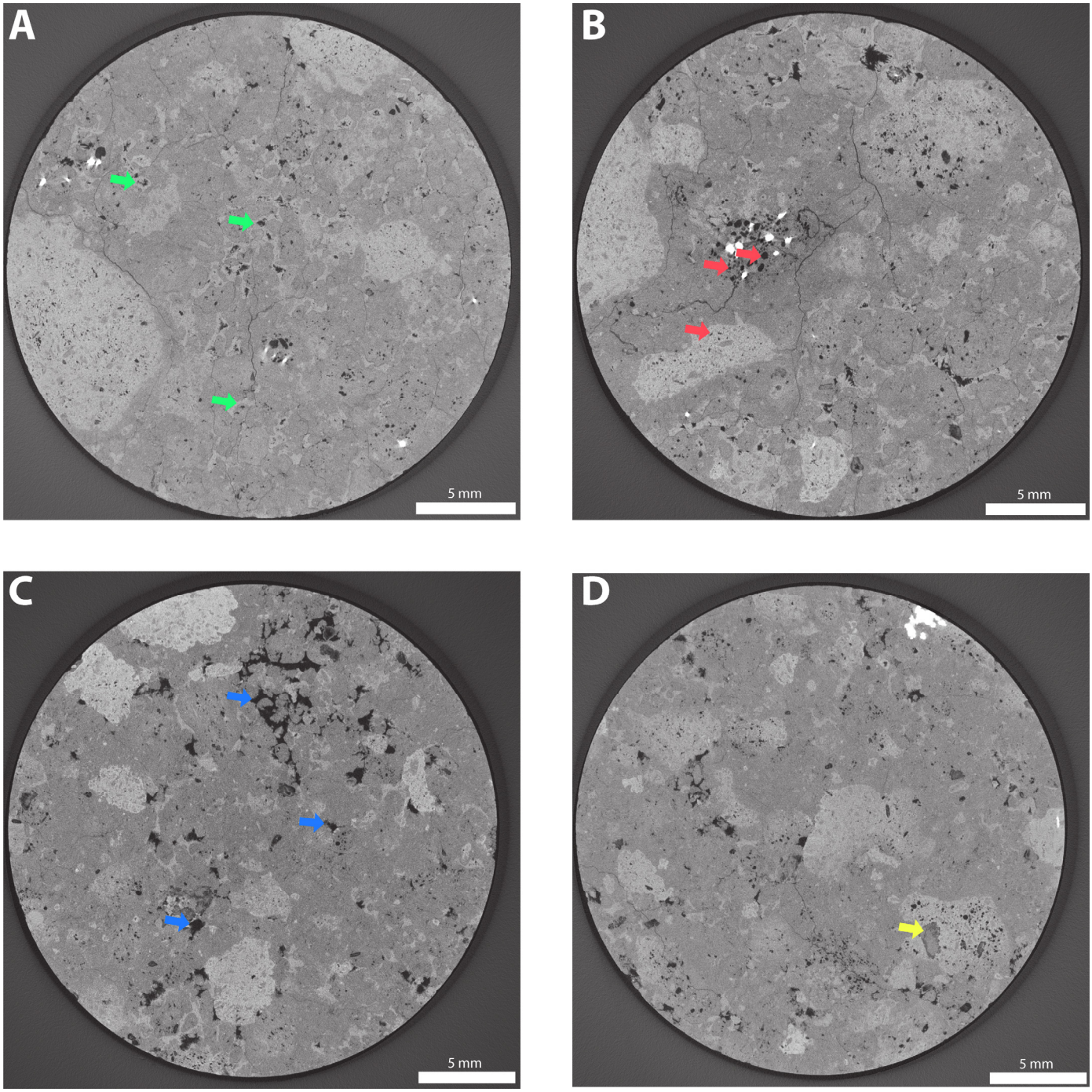

Figure 6. X–ray computed tomography scanned slices (13.2 µm voxels), 1-inch-diameter × several-inches-in-length core plugs. Note variability between lapilli and between slices. Dark areas = open pores. Some very bright grains are relict intermediate ferrochromite-spinel and some are sulfides. Medium-gray areas predominantly either smectite or vermiculite. Slightly brighter lapilli are partly altered to various Ca–Ti silicates. Each sample has ~29% porosity. (A) Slice in which most interparticle pore space filled with fibrous pectolite cement (slightly lighter gray) (green arrows). Note induced microfractures. From 2219.3 ft (676.4 m). (B) Slice showing abundant lapilli containing vesicles (red arrows). Note induced microfractures. From 2219.3 ft (676.4 m). (C) Slice with open interparticle pores (blue arrows). Note induced microfractures. From 2291.8 ft (698.5 m). (D) Slice with mix of pore types, including large phenocryst (yellow arrow) altered to vermiculite and smectite. Note induced microfractures. From 2291.8 ft (698.5 m).

REFERENCES CITED

Barker, D. S., R. H. Mitchell, and D. McKay, 1987, Late Cretaceous nephelinite to phonolite magmatism in the Balcones Province, Texas: Geological Society of America Special Paper 215, Boulder, Colorado, p. 293–304, <https://doi.org/10.1130/spe215-p293>.

Barker, D. S., and K. P. Young, 1979, A marine Cretaceous nepheline basanite volcano at Austin, Texas: Texas Journal of Science, v. 31, p. 5–24.

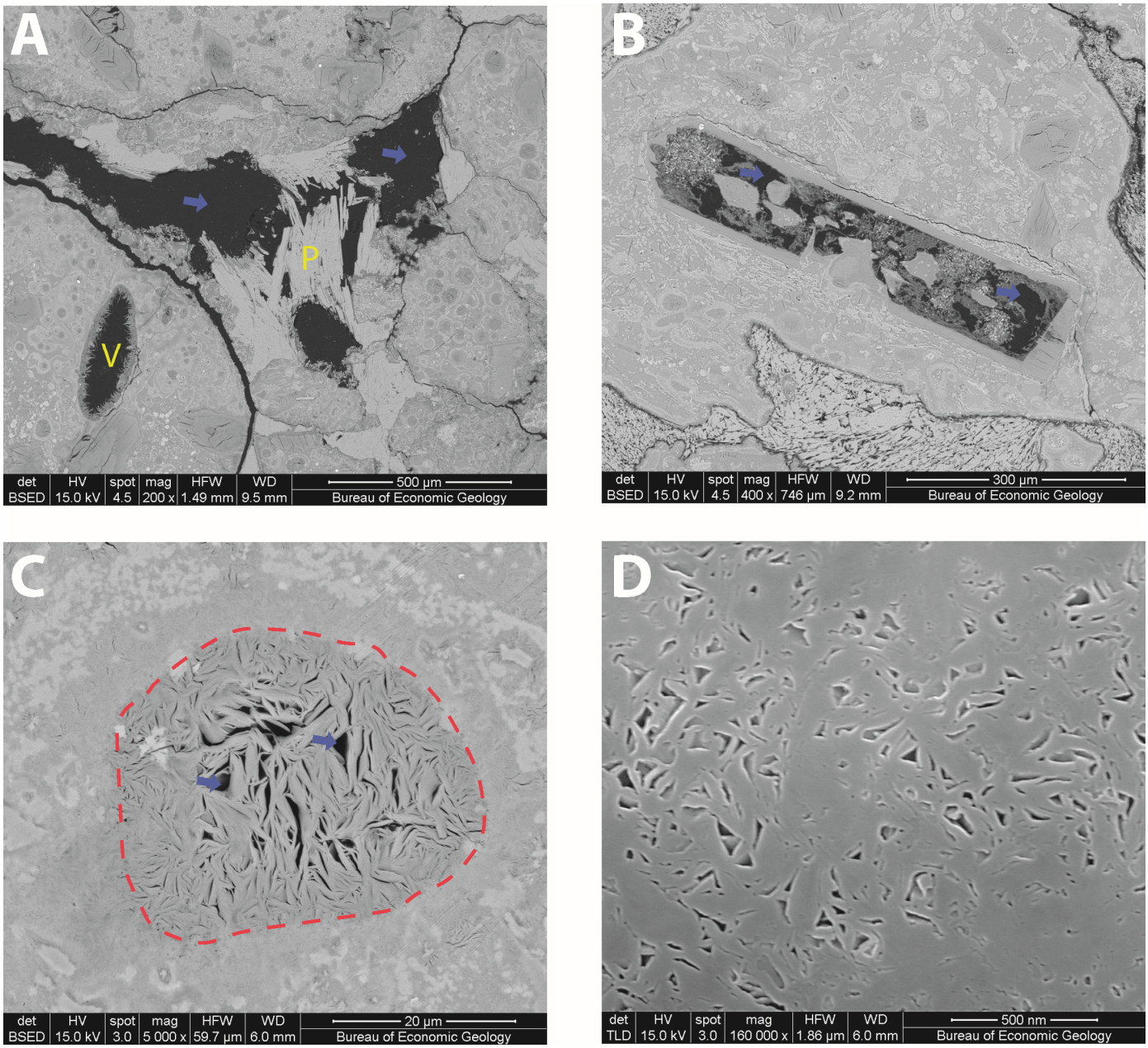

Figure 7. SEM images of pore types in tuffs; dark areas are pores. (A) BSE image showing in center partly cemented interparticle pore space (blue arrows) between lapilli. Light-gray bladed crystals are pectolite (yellow P) cement filling in interparticle pore space. Lower right has vesicle (yellow V) partly filled by smectite. Polished thin section from 2219.3 ft (676.4 m). (B) BSE image showing partly replaced phenocryst with intraparticle pores (blue arrows) within lapilli. Phenocryst replaced primarily by vermiculite/smectite with minor amounts of bladed xonotlite. Polished thin section from 2268.3 ft (691.4 m). Paired low-magnification (C) and high-magnification (D) SEM images. BSE image on left showing view of vesicle (outlined in red) filled mostly with smectite (blue arrows point to intraparticle pores) and altered matrix surrounding it. SE image on right shows high magnification view of matrix, revealing that it has been altered to fine-grained phyllosilicate minerals, probably mostly interlayered vermiculite/smectite. Note abundant nanometer-scale pores, which contribute significantly to total porosity. Ar–ion milled surface from 2290.9 ft (698.3 m).

Condon, S. M., and T. S. Dyman, 2006, Chapter 2: 2003 geologic assessment of undiscovered conventional oil and gas resources in the Upper Cretaceous Navarro and Taylor groups, western Gulf Province, Texas, *in* U.S. Geological Survey Western Gulf Province Assessment Team, Petroleum systems and geologic assessment of undiscovered oil and gas, Navarro and Taylor groups, western Gulf Province, Texas: U.S. Geological Survey Digital Data Series 69–H, 47 p., <https://pubs.usgs.gov/dds/dds-069/dds-069-h/REPORTS/69_H_CH_2.pdf>.

Ewing, T. E., 1986, Balcones volcanoes in South Texas–exploration methods and examples, *in* W. L. Stapp, ed., Contributions to the Geology of South Texas, South Texas Geological Society, San Antonio, p. 368–379.

Ewing, T. E., and S. C. Caran, 1982, Late Cretaceous volcanism in South and Central Texas; Stratigraphic, structural, and seismic

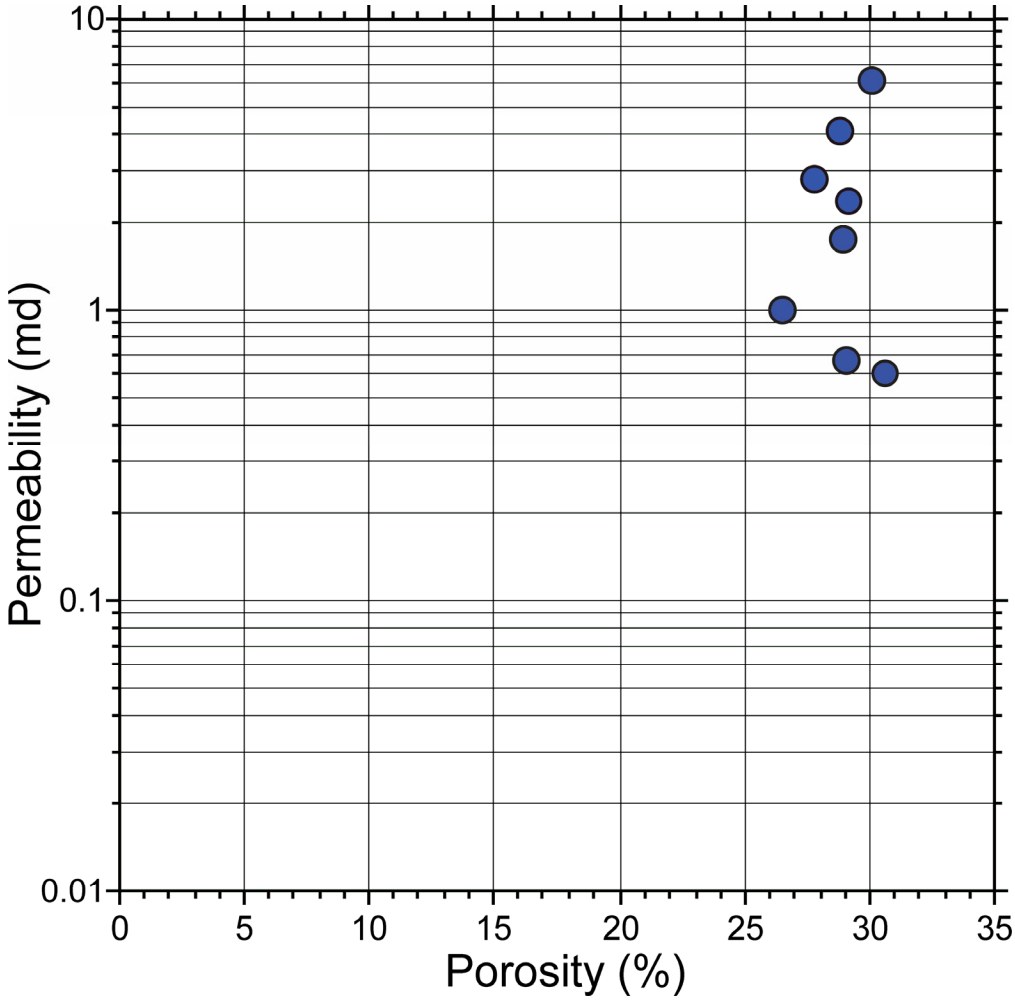

Figure 8. Plot of porosity versus permeability showing lack of linear relationship between two parameters. As noted in text, permeability values probably influenced by induced fractures and values unreliable. However, porosity values appear accurate on the basis of comparison with MICP and NMR analyses.

models: Gulf Coast Association of Geological Societies Transactions, v. 32, p. 137–145.

Griffin, W. R., K. A. Foland, R. J. Stern, and M. I. Leybourne, 2010, Geochronology of bimodal alkaline volcanism in the Balcones Igneous Province, Texas: Implications for Cretaceous intraplate magmatism in the northern Gulf of Mexico magmatic zone: Journal of Geology, v. 118, p. 1–21, <https://doi.org/10.1086/648532>.

Hutchinson, P. J., 1994, Upper Cretaceous (Austin Group) volcanic deposits as a hydrocarbon trap: Gulf Coast Association of Geological Societies Transactions, v. 44, p. 213–225.

Lonsdale, J. T., 1927, Igneous rocks of the Balcones Fault region of Texas: University of Texas at Austin Bulletin 2744, 178 p.

Loucks, R. G., J. R. Lambert, K. Patty, T. E. Larson, R. M. Reed, and C. K. Zahm, 2020, Regional overview and significance of the mineralogy of the Upper Cretaceous Austin Chalk Group, onshore Gulf of Mexico: Gulf Coast Association of Geological Societies Journal, v. 9, p. 1–16, <https://www.gcags.org/Journal/2020.GCAGS.Journal/2020.GCAGS.Journal.v9.01.p1-16.Loucks.et.al.pdf>.

Loucks, R. G., and R. M. Reed, 2022, Characterization of volcanic-induced, carbonate mass-wasting complexes in the Upper Cretaceous (early Campanian) Austin Chalk strata in the Maverick Basin and San Marcos Arch areas of South and Central Texas, USA: Sedimentary Geology, v. 432, Paper 106120, 18 p., <https://doi.org/10.1016/j.sedgeo.2022.106120>.

Luttrell, P. E., 1977, Carbonate facies distribution and diagenesis associated with volcanic cones—Anacacho Limestone (Upper Cretaceous), Elaine Field, Dimmit County, Texas, *in* D. G. Bebout and R. G. Loucks, eds., Cretaceous carbonates of Texas and Mexico: Applications to subsurface exploration: Bureau of Economic Geology Report of Investigations 89, Austin, Texas, p. 260–285.

Ogiesoba, O. C., and R. L. Eastwood, 2013, Seismic multiattribute analysis for shale gas/oil within the Austin Chalk and Eagle Ford Shale in a submarine volcanic terrain, Maverick Basin, South Texas: Interpretation, v. 1, p. SB61–SB83, <https://doi.org/10.1190/INT-2013-0019.1>.

Ogiesoba, O. C., and A. Klokov, 2017, Examples of seismic diffraction imaging from the Austin Chalk and Eagle Ford Shale, Maverick Basin, South Texas: Journal of Petroleum Science and Engineering, v. 157, p. 248–263, <https://doi.org/10.1016/j.petrol.2017.07.040>.

Phelps, R. M., C. Kerans, R. G. Loucks, R. O. B. P. Da Gama, J. Jeremiah, and D. Hull, 2013, Oceanographic and eustatic control of carbonate platform evolution and sequence stratigraphy on the Cretaceous (Valanginian-Campanian) passive margin, northern Gulf of Mexico: Sedimentology, v. 62, p. 461–496, <https://doi.org/10.1111/sed.12062>.

Reed, R. M., R. G. Loucks, and R. Adriaens, 2022, Mineralogy, alteration, fabric, and texture of silica-undersaturated mafic lapilli tuffs from the Late Cretaceous Balcones Igneous Province, Central Texas, USA (abs.): Geological Society of America Abstracts with Programs, v. 54, no. 5, 1 p., <http://doi.org/10.1130/abs/2022AM-378153>.

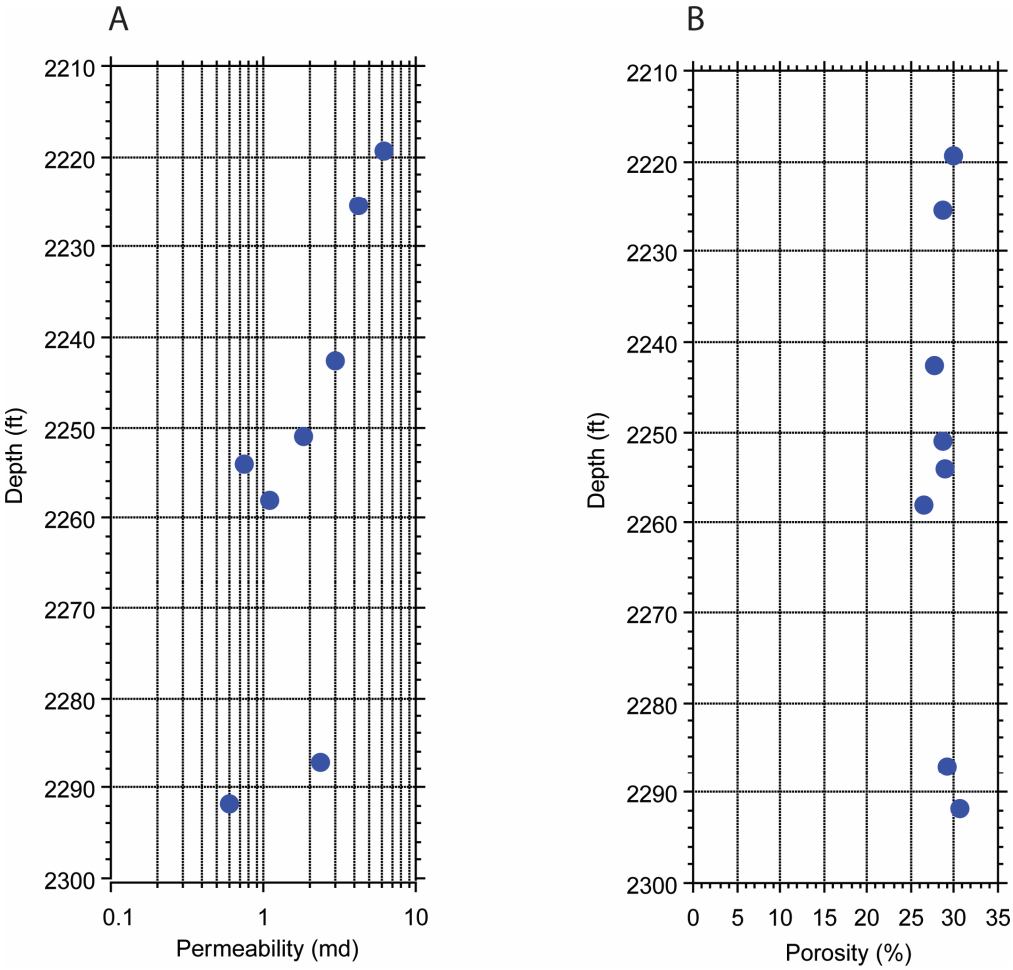

Figure 9. (A) Plot of permeability versus depth, showing weak negative correlation with increasing depth. (B) Plot of porosity versus depth showing no correlation over short depth interval.

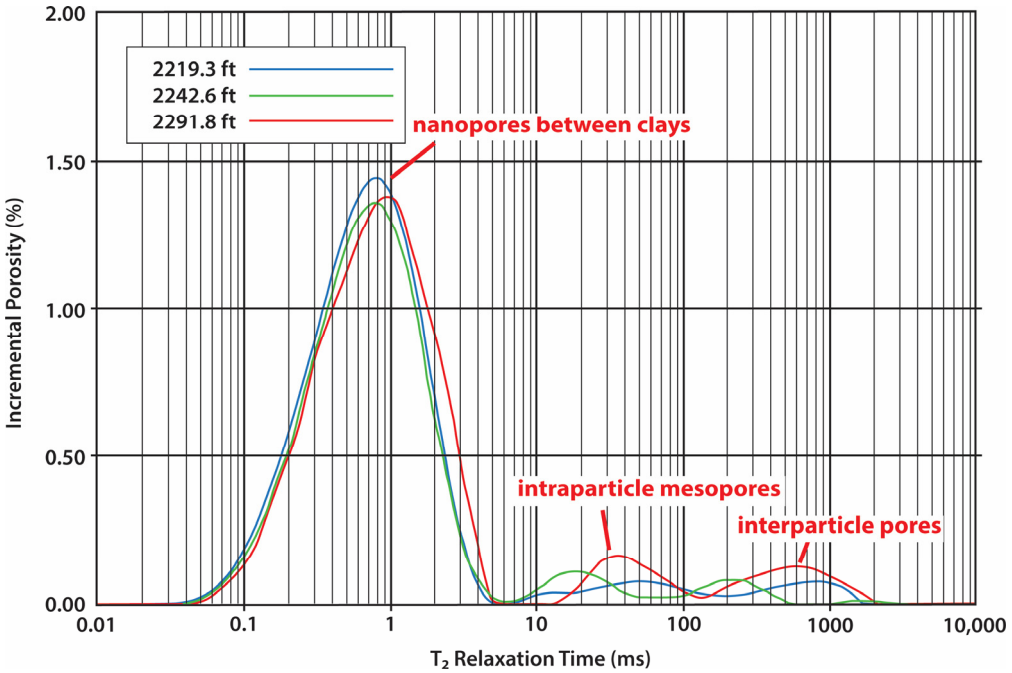

Figure 10. Plot showing NMR curves of three core plugs. All three samples show similar responses. Labels relative to pore sizes based on interpretation from thin sections and SEM samples.

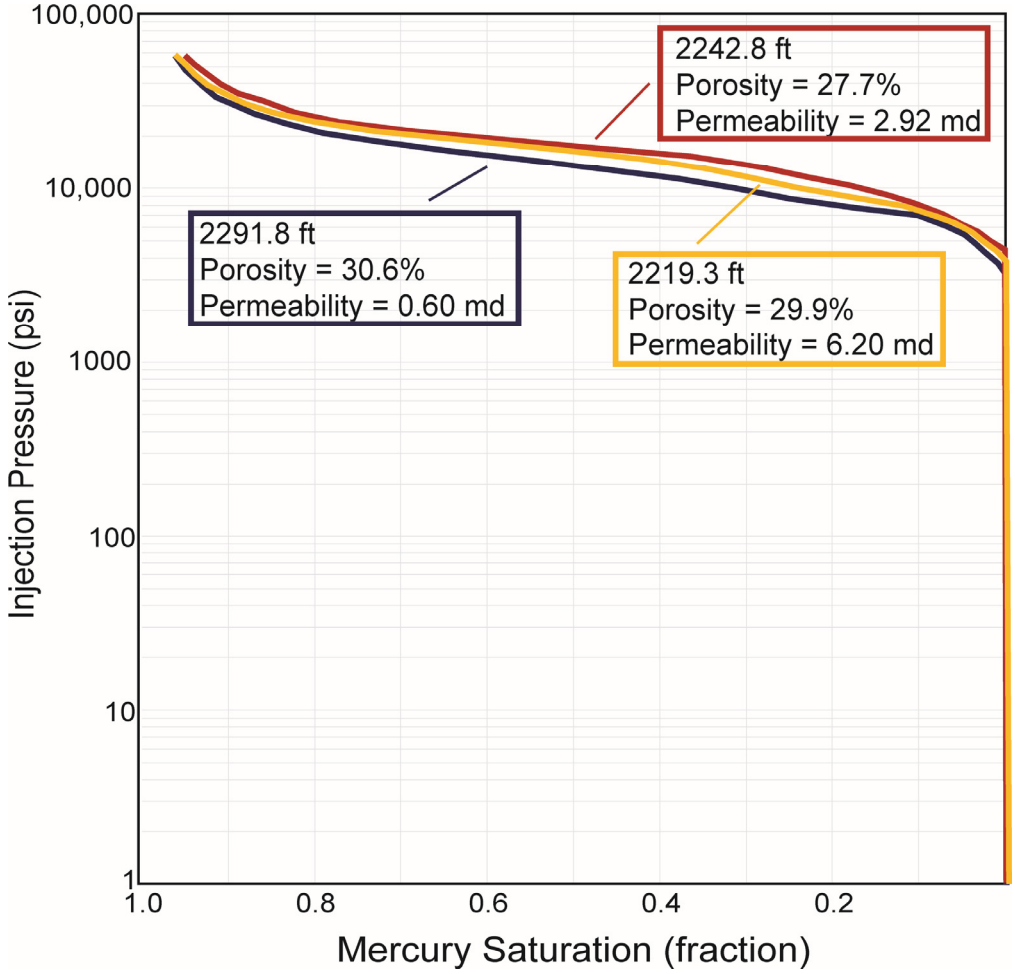

Figure 11. MICP curves. All three sample show similar curve morphology with high entry pressures ~4000 psi (~27.6 MPa). 1000 psi = ~6.89 MPa.

Sellards, E. H., 1932, Oil fields in igneous rocks in coastal plain of Texas: American Association of Petroleum Geologists Bulletin, v. 16, p. 741–768, <https://doi.org/10.1306/3d932aba-16b1-11d7-8645000102c1865d>.

Shuster, M. W., C. K. Zahm, and P. H. Hennings, 2021, Oil and gas in fractured crystalline igneous and metamorphic rocks: Global overview and examples from Texas, *in* O. A. Callahan and P. Eichhubl, eds., The geologic basement of Texas: A volume in honor of Peter T. Flawn: Bureau of Economic Geology Report of Investigations 286, Austin, Texas, 68 p., <https://doi.org/ 10.23867/RI0286C3>.

Spencer, A. B., 1969, Alkalic igneous rocks of the Balcones Province, Texas: Journal of Petrology, v. 10, p. 272–306, <https://doi.org/10.1093/petrology/10.2.272>.

Thompson, M. E., 1986. Stratigraphy of the Dale Lime and its relation to structure at Bateman Field, Bastrop County, Texas: South Texas Geological Society Bulletin, v. 34, p. 356–367.

Thompson, M. E., 2019, A revised age range for Texas Gulf Coast serpentine mounds: South Texas Geological Society Bulletin, v. 60, p. 19–33.

Udden, J. A., and H. P. Bybee, 1916, The Thrall Oil Field: University of Texas Bulletin 66, Austin, 66 p.

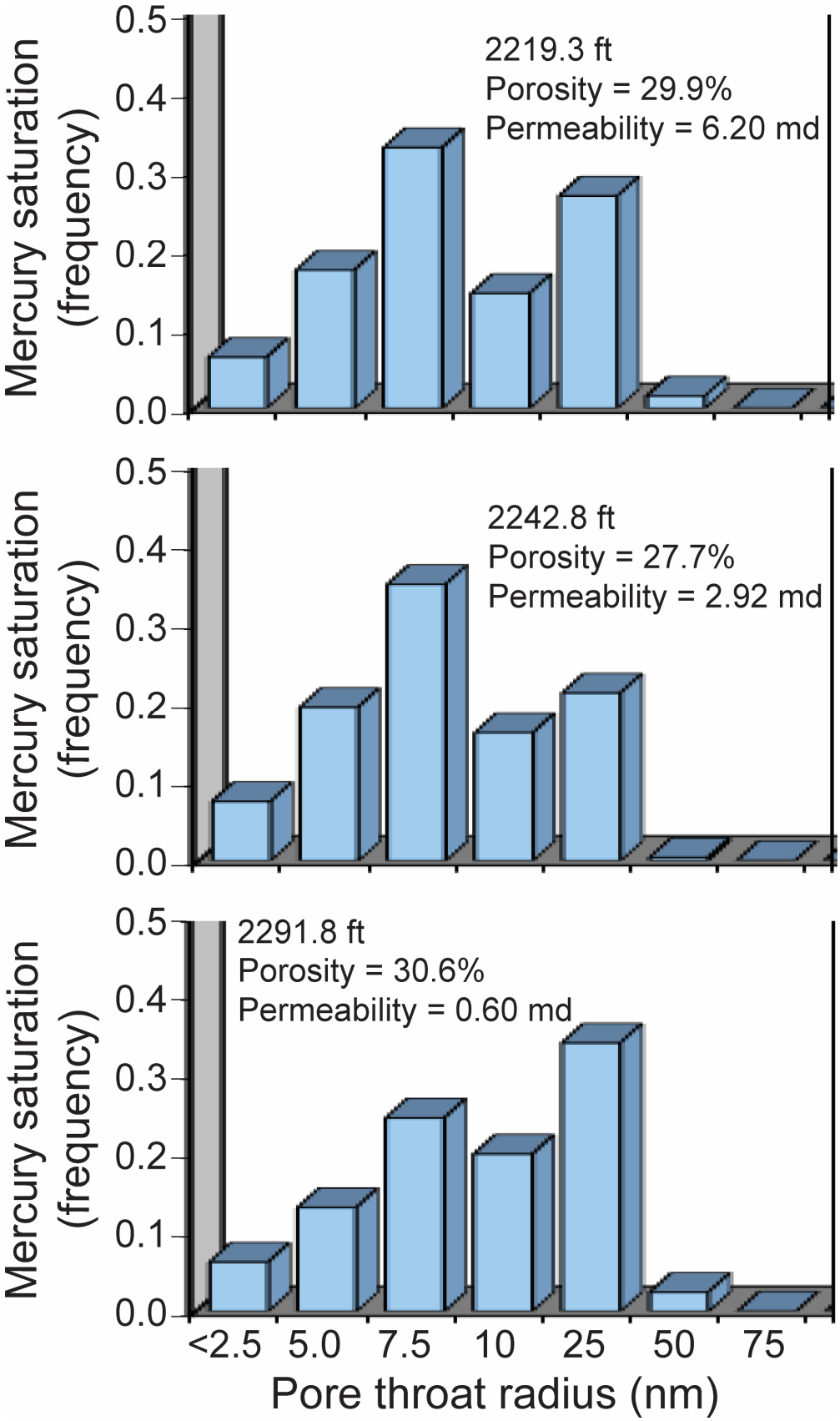

Figure 12. Pore-throat-radius frequency in nanometers calculated from MICP analysis. Each sample has essentially same pore-throat-radius distribution. All pore throats in nanopore throat range.